

Study of $e^+e^- \rightarrow B^{(*)}\bar{B}^{(*)}\pi^\pm$ at $\sqrt{s} = 10.866$ GeV

A. Garmash,^{3,47} A. Abdesselam,⁵⁷ I. Adachi,^{13,10} H. Aihara,⁶² D. M. Asner,⁴⁹ T. Aushev,^{38,22} R. Ayad,⁵⁷ T. Aziz,⁵⁸ V. Babu,⁵⁸ I. Badhrees,^{57,27} A. M. Bakich,⁵⁶ P. Behera,¹⁷ V. Bhardwaj,⁵⁴ B. Bhuyan,¹⁶ A. Bobrov,^{3,47} A. Bondar,^{3,47} G. Bonvicini,⁶⁷ A. Bozek,⁴⁵ M. Bračko,^{34,23} T. E. Browder,¹² D. Červenkov,⁴ V. Chekelian,³⁵ A. Chen,⁴² B. G. Cheon,¹¹ K. Chilikin,²² K. Cho,²⁸ V. Chobanova,³⁵ Y. Choi,⁵⁵ D. Cinabro,⁶⁷ J. Dalseno,^{35,59} M. Danilov,^{22,37} N. Dash,¹⁵ Z. Doležal,⁴ A. Drutskoy,^{22,37} D. Dutta,⁵⁸ S. Eidelman,^{3,47} D. Epifanov,⁶² H. Farhat,⁶⁷ J. E. Fast,⁴⁹ T. Ferber,⁷ B. G. Fulsom,⁴⁹ V. Gaur,⁵⁸ N. Gabyshev,^{3,47} R. Gillard,⁶⁷ Y. M. Goh,¹¹ P. Goldenzweig,²⁵ B. Golob,^{32,23} T. Hara,^{13,10} K. Hayasaka,⁴⁰ H. Hayashii,⁴¹ T. Iijima,^{40,39} A. Ishikawa,⁶⁰ R. Itoh,^{13,10} Y. Iwasaki,¹³ I. Jaegle,¹² D. Joffe,²⁶ K. K. Joo,⁵ T. Julius,³⁶ K. H. Kang,³⁰ E. Kato,⁶⁰ T. Kawasaki,⁴⁶ D. Y. Kim,⁵³ J. B. Kim,²⁹ K. T. Kim,²⁹ M. J. Kim,³⁰ S. H. Kim,¹¹ Y. J. Kim,²⁸ K. Kinoshita,⁶ S. Korpar,^{34,23} P. Križan,^{32,23} P. Krokovny,^{3,47} A. Kuzmin,^{3,47} Y.-J. Kwon,⁶⁹ J. S. Lange,⁹ I. S. Lee,¹¹ C. Li,³⁶ H. Li,¹⁸ L. Li,⁵¹ L. Li Gioi,³⁵ J. Libby,¹⁷ D. Liventsev,^{66,13} P. Lukin,^{3,47} M. Masuda,⁶¹ D. Matvienko,^{3,47} K. Miyabayashi,⁴¹ H. Miyata,⁴⁶ R. Mizuk,^{22,37} G. B. Mohanty,⁵⁸ A. Moll,^{35,59} T. Mori,³⁹ R. Mussa,²¹ E. Nakano,⁴⁸ M. Nakao,^{13,10} T. Nanut,²³ Z. Natkaniec,⁴⁵ S. Nishida,^{13,10} S. L. Olsen,⁵² P. Pakhlov,^{22,37} G. Pakhlova,^{38,22} B. Pal,⁶ H. Park,³⁰ T. K. Pedlar,³³ R. Pestotnik,²³ M. Petrič,²³ L. E. Piiilonen,⁶⁶ C. Pulvermacher,²⁵ E. Ribežl,²³ M. Ritter,³⁵ A. Rostomyan,⁷ H. Sahoo,¹² Y. Sakai,^{13,10} S. Sandilya,⁵⁸ T. Sanuki,⁶⁰ V. Savinov,⁵⁰ O. Schneider,³¹ G. Schnell,^{1,14} C. Schwanda,²⁰ Y. Seino,⁴⁶ D. Semmler,⁹ K. Senyo,⁶⁸ I. S. Seong,¹² M. E. Sevir,³⁶ V. Shebalin,^{3,47} C. P. Shen,² T.-A. Shibata,⁶³ J.-G. Shiu,⁴⁴ B. Shwartz,^{3,47} F. Simon,^{35,59} Y.-S. Sohn,⁶⁹ E. Solovieva,²² M. Starič,²³ T. Sumiyoshi,⁶⁴ U. Tamponi,^{21,65} K. Tanida,⁵² Y. Teramoto,⁴⁸ K. Trabelsi,^{13,10} M. Uchida,⁶³ S. Uehara,^{13,10} T. Uglov,^{22,38} S. Uno,^{13,10} C. Van Hulse,¹ P. Vanhoefer,³⁵ G. Varner,¹² V. Vorobyev,^{3,47} M. N. Wagner,⁹ C. H. Wang,⁴³ M.-Z. Wang,⁴⁴ P. Wang,¹⁹ Y. Watanabe,²⁴ K. M. Williams,⁶⁶ E. Won,²⁹ H. Yamamoto,⁶⁰ J. Yamaoka,⁴⁹ S. Yashchenko,⁷ J. Yelton,⁸ Y. Yook,⁶⁹ C. Z. Yuan,¹⁹ Z. P. Zhang,⁵¹ V. Zhilich,^{3,47} V. Zhulanov,^{3,47} and A. Zupanc²³

(The Belle Collaboration)

¹University of the Basque Country UPV/EHU, 48080 Bilbao

²Beihang University, Beijing 100191

³Budker Institute of Nuclear Physics SB RAS, Novosibirsk 630090

⁴Faculty of Mathematics and Physics, Charles University, 121 16 Prague

⁵Chonnam National University, Kwangju 660-701

⁶University of Cincinnati, Cincinnati, Ohio 45221

⁷Deutsches Elektronen-Synchrotron, 22607 Hamburg

⁸University of Florida, Gainesville, Florida 32611

⁹Justus-Liebig-Universität Gießen, 35392 Gießen

¹⁰SOKENDAI (The Graduate University for Advanced Studies), Hayama 240-0193

¹¹Hanyang University, Seoul 133-791

¹²University of Hawaii, Honolulu, Hawaii 96822

¹³High Energy Accelerator Research Organization (KEK), Tsukuba 305-0801

¹⁴IKERBASQUE, Basque Foundation for Science, 48013 Bilbao

¹⁵Indian Institute of Technology Bhubaneswar, Satya Nagar 751007

¹⁶Indian Institute of Technology Guwahati, Assam 781039

¹⁷Indian Institute of Technology Madras, Chennai 600036

¹⁸Indiana University, Bloomington, Indiana 47408

¹⁹Institute of High Energy Physics, Chinese Academy of Sciences, Beijing 100049

²⁰Institute of High Energy Physics, Vienna 1050

²¹INFN - Sezione di Torino, 10125 Torino

²²Institute for Theoretical and Experimental Physics, Moscow 117218

²³J. Stefan Institute, 1000 Ljubljana

²⁴Kanagawa University, Yokohama 221-8686

²⁵Institut für Experimentelle Kernphysik, Karlsruher Institut für Technologie, 76131 Karlsruhe

²⁶Kennesaw State University, Kennesaw GA 30144

²⁷King Abdulaziz City for Science and Technology, Riyadh 11442

²⁸Korea Institute of Science and Technology Information, Daejeon 305-806

²⁹Korea University, Seoul 136-713

³⁰Kyungpook National University, Daegu 702-701

³¹École Polytechnique Fédérale de Lausanne (EPFL), Lausanne 1015

- ³²Faculty of Mathematics and Physics, University of Ljubljana, 1000 Ljubljana
³³Luther College, Decorah, Iowa 52101
³⁴University of Maribor, 2000 Maribor
³⁵Max-Planck-Institut für Physik, 80805 München
³⁶School of Physics, University of Melbourne, Victoria 3010
³⁷Moscow Physical Engineering Institute, Moscow 115409
³⁸Moscow Institute of Physics and Technology, Moscow Region 141700
³⁹Graduate School of Science, Nagoya University, Nagoya 464-8602
⁴⁰Kobayashi-Maskawa Institute, Nagoya University, Nagoya 464-8602
⁴¹Nara Women's University, Nara 630-8506
⁴²National Central University, Chung-li 32054
⁴³National United University, Miao Li 36003
⁴⁴Department of Physics, National Taiwan University, Taipei 10617
⁴⁵H. Niewodniczanski Institute of Nuclear Physics, Krakow 31-342
⁴⁶Niigata University, Niigata 950-2181
⁴⁷Novosibirsk State University, Novosibirsk 630090
⁴⁸Osaka City University, Osaka 558-8585
⁴⁹Pacific Northwest National Laboratory, Richland, Washington 99352
⁵⁰University of Pittsburgh, Pittsburgh, Pennsylvania 15260
⁵¹University of Science and Technology of China, Hefei 230026
⁵²Seoul National University, Seoul 151-742
⁵³Soongsil University, Seoul 156-743
⁵⁴University of South Carolina, Columbia, South Carolina 29208
⁵⁵Sungkyunkwan University, Suwon 440-746
⁵⁶School of Physics, University of Sydney, NSW 2006
⁵⁷Department of Physics, Faculty of Science, University of Tabuk, Tabuk 71451
⁵⁸Tata Institute of Fundamental Research, Mumbai 400005
⁵⁹Excellence Cluster Universe, Technische Universität München, 85748 Garching
⁶⁰Tohoku University, Sendai 980-8578
⁶¹Earthquake Research Institute, University of Tokyo, Tokyo 113-0032
⁶²Department of Physics, University of Tokyo, Tokyo 113-0033
⁶³Tokyo Institute of Technology, Tokyo 152-8550
⁶⁴Tokyo Metropolitan University, Tokyo 192-0397
⁶⁵University of Torino, 10124 Torino
⁶⁶CNP, Virginia Polytechnic Institute and State University, Blacksburg, Virginia 24061
⁶⁷Wayne State University, Detroit, Michigan 48202
⁶⁸Yamagata University, Yamagata 990-8560
⁶⁹Yonsei University, Seoul 120-749

We report the analysis of the three-body $e^+e^- \rightarrow B\bar{B}\pi$, $B\bar{B}^*\pi$, and $B^*\bar{B}^*\pi$ processes, including the first observation of the $Z_b^\pm(10610) \rightarrow [B\bar{B}^* + \text{c.c.}]^\pm$ and $Z_b^\pm(10650) \rightarrow [B^*\bar{B}^*]^\pm$ transitions. We measure visible cross sections for the three-body production of $\sigma_{\text{vis}}(e^+e^- \rightarrow [B\bar{B}^* + \text{c.c.}]^\pm\pi^\mp) = (11.2 \pm 1.0(\text{stat.}) \pm 1.2(\text{syst.}))$ pb and $\sigma_{\text{vis}}(e^+e^- \rightarrow [B^*\bar{B}^*]^\pm\pi^\mp) = (5.61 \pm 0.73(\text{stat.}) \pm 0.66(\text{syst.}))$ pb and set a 90% C.L. upper limit of $\sigma_{\text{vis}}(e^+e^- \rightarrow [B\bar{B}]^\pm\pi^\mp) < 2.1$ pb. The results are based on a 121.4 fb^{-1} data sample collected with the Belle detector at a center-of-mass energy near the $\Upsilon(10860)$ peak.

PACS numbers: 14.40.Rt, 14.40.Pq, 13.66.Bc

Two new charged bottomonium-like resonances, $Z_b(10610)$ and $Z_b(10650)$, have been observed recently by the Belle Collaboration in $e^+e^- \rightarrow \Upsilon(nS)\pi^+\pi^-$, $n = 1, 2, 3$ and $e^+e^- \rightarrow h_b(mP)\pi^+\pi^-$, $m = 1, 2$ [1, 2]. Analysis of the quark composition of the initial and final states reveals that these hadronic objects have an exotic nature: Z_b should be comprised of (at least) four quarks including a $b\bar{b}$ pair. Several models [3] have been proposed to describe the internal structure of these states. In Ref. [4], it was suggested that $Z_b(10610)$ and $Z_b(10650)$ states might be loosely bound $B\bar{B}^*$ and $B^*\bar{B}^*$ systems, respectively. If so, it is natural to expect the Z_b states

to decay to final states with $B^{(*)}$ mesons at substantial rates.

Evidence for the three-body $\Upsilon(10860) \rightarrow B\bar{B}^*\pi$ decay has been reported previously by Belle, based on a data sample of 23.6 fb^{-1} [5]. In this analysis, we use a data sample with an integrated luminosity of 121.4 fb^{-1} collected near the peak of the $\Upsilon(10860)$ resonance ($\sqrt{s} = 10.866 \text{ GeV}$) with the Belle detector [6] at the KEKB asymmetric-energy e^+e^- collider [7]. Note that we reconstruct only three-body $B^{(*)}\bar{B}^{(*)}\pi$ combinations with a charged primary pion. For brevity, we adopt the following notations: the set of $B^+\bar{B}^0\pi^-$ and

$B^- B^0 \pi^+$ final states is referred to as $BB\pi$; the set of $B^+ \bar{B}^0 \pi^-$, $B^- B^0 \pi^+$, $B^0 B^{*-} \pi^+$ and $\bar{B}^0 B^{*+} \pi^-$ final states is referred to as $BB^* \pi$; and the set of $B^{*+} \bar{B}^0 \pi^-$ and $B^{*-} B^0 \pi^+$ final states is denoted as $B^* B^* \pi$. The inclusion of the charge conjugate mode is implied throughout this report.

We use Monte Carlo (MC) events generated with EvtGen [8] and then processed through a detailed detector simulation implemented in GEANT3 [9]. Final-state radiation from charged particles is simulated during event generation using PHOTOS [10]. The simulated samples for $e^+e^- \rightarrow q\bar{q}$ ($q = u, d, s, c$, or b) are equivalent to six times the integrated luminosity of the data and are used to develop criteria to separate signal events from backgrounds, identify types of background events, determine the reconstruction efficiency and parameterize the distributions needed for the extraction of the signal decays.

B mesons are reconstructed in the following decay channels: $B^+ \rightarrow J/\psi K^{(*)+}$, $B^+ \rightarrow \bar{D}^{(*)0} \pi^+$, $B^0 \rightarrow J/\psi K^{(*)0}$, $B^0 \rightarrow D^{(*)-} \pi^+$ (eighteen in total). Charged-track candidates are required to be consistent with origination from the interaction point (IP). A likelihood ratio for a given track to be a π , K , or p is obtained by utilizing energy-loss measurements in the (CDC), light yield measurements from an array of aerogel threshold Cherenkov counters, and time-of-flight information from a barrel-like arrangement of time-of-flight scintillation counters. Photons are detected with an electromagnetic calorimeter (ECL) and are required to have energies in the laboratory frame of at least 50 (100) MeV in the ECL barrel (endcaps) and not be associated with charged tracks.

Neutral pion candidates are reconstructed using photon pairs with an invariant mass between 120 and 150 MeV/ c^2 . Neutral kaon candidates are reconstructed using pairs of oppositely-charged pions with an invariant mass within 15 MeV/ c^2 of the nominal K^0 mass. The direction of the K^0 candidate momentum vector is required to be consistent with the direction of its vertex displacement relative to the IP. The K^{*0} (K^{*+}) is reconstructed in the $K^+ \pi^-$ ($K^0 \pi^+$) final state, the invariant mass of the K^* candidate is required to be within 150 MeV/ c^2 of the nominal K^* mass [11]. The invariant mass of a $J/\psi \rightarrow \ell^+ \ell^-$ candidate is required to be within 30 (50) MeV/ c^2 for $\ell = e$ (μ), of the nominal J/ψ mass. Neutral (charged) D mesons are reconstructed in the $K^- \pi^+$, $K^- \pi^+ \pi^0$, and $K^- \pi^- \pi^+ \pi^+$ ($K^- \pi^+ \pi^+$) modes. To identify D^* candidates, we require $|M(D\pi) - M(D) - \Delta m_{D^*}| < 3$ MeV/ c^2 , where $M(D\pi)$ and $M(D)$ are the reconstructed masses of the D^* and D candidates, respectively, and $\Delta m_{D^*} = m_{D^*} - m_D$ is the difference between the nominal D^* and D masses. The mass windows for narrow states quoted above correspond to a $\pm 2.5\sigma$ requirement.

The dominant background comes from $e^+e^- \rightarrow c\bar{c}$ continuum events, where true D mesons produced in e^+e^- annihilation are combined with random particles to form

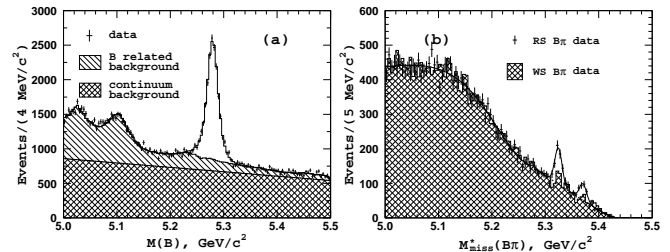


FIG. 1. The (a) invariant mass and (b) $M_{\text{miss}}^*(B\pi)$ distribution for B candidates in the B signal region. Points with error bars represent the data. The open histogram in (a) shows the result of the fit to data. The solid line in (b) shows the result of the fit to the RS $B\pi$ data; the dashed line represents the background level.

a B candidate. This type of background is suppressed using variables that characterize the event topology. Since the momenta of the two B mesons produced from a three-body $e^+e^- \rightarrow B^{(*)} B^{(*)} \pi$ decay are low in the c.m. frame (below 0.9 GeV/ c), their decay products are essentially uncorrelated so that the event tends to be spherical. In contrast, hadrons from continuum events tend to exhibit a back-to-back jet structure. We use θ_{thr} , the angle between the thrust axis of the B candidate and that of the rest of the event, to discriminate between the two cases. The distribution of $|\cos \theta_{\text{thr}}|$ is strongly peaked near $|\cos \theta_{\text{thr}}| = 1.0$ for $c\bar{c}$ events and is nearly flat for $B^{(*)} B^{(*)} \pi$ events. We require $|\cos \theta_{\text{thr}}| < 0.80$ for the $B \rightarrow D^{(*)} \pi$ final states; this eliminates about 81% of the continuum background and retains 73% of the signal events.

We identify B candidates by their reconstructed invariant mass $M(B)$ and momentum $P(B)$ in the center-of-mass (c.m.) frame. We require $P(B) < 1.35$ GeV/ c to retain B mesons produced in both two-body and multi-body processes. The $M(B)$ distribution for B candidates is shown in Fig. 1(a). We perform a binned maximum likelihood fit of the $M(B)$ distribution to the sum of a signal component parameterized by a Gaussian function and two background components: one related to other decay modes of B mesons and one due to continuum $e^+e^- \rightarrow q\bar{q}$ processes, where $q = u, d, s, c$. The shape of the B -related background is determined from a large sample of generic MC; the shape of the $q\bar{q}$ background is parameterized with a linear function. The parameters of the signal Gaussian, the normalization of the B -related background and the parameters of the $q\bar{q}$ background float in the fit. We find 12263 ± 168 fully reconstructed B mesons. The B signal region is defined by requiring $M(B)$ to be within 30 to 40 MeV/ c^2 (depending on the B decay mode) of the nominal B mass.

Reconstructed B^+ or \bar{B}^0 candidates are combined with π^- 's — the right-sign (RS) combination — and the missing mass, $M_{\text{miss}}(B\pi)$, is calculated as $M_{\text{miss}}(B\pi) =$

$\sqrt{(\sqrt{s} - E_{B\pi})^2/c^4 - P_{B\pi}^2/c^2}$, where $E_{B\pi}$ and $P_{B\pi}$ are the measured energy and momentum of the reconstructed $B\pi$ combination. Signal $e^+e^- \rightarrow BB^*\pi$ events produce a narrow peak in the $M_{\text{miss}}(B\pi)$ spectrum around the nominal B^* mass while $e^+e^- \rightarrow B^*B^*\pi$ events produce a peak at $m_{B^*} + \Delta m_{B^*}$, where $\Delta m_{B^*} = m_{B^*} - m_B$, due to the missed photon from the $B^* \rightarrow B\gamma$ decay. It is important to note here that, according to signal MC, $BB^*\pi$ events, where the reconstructed B is the one from the B^* , produce a peak in the $M_{\text{miss}}(B\pi)$ distribution at virtually the same position as $BB^*\pi$ events, where the reconstructed B is the primary one. To remove the correlation between $M_{\text{miss}}(B\pi)$ and $M(B)$ and to improve the resolution, we use $M_{\text{miss}}^* = M_{\text{miss}}(B\pi) + M(B) - m_B$ instead of $M_{\text{miss}}(B\pi)$. The M_{miss}^* distribution for the RS combinations is shown in Fig. 1(b), where peaks corresponding to the $BB^*\pi$ and $B^*B^*\pi$ signals are evident. Combinations with π^+ — the wrong sign (WS) combinations — are used to evaluate the shape of the combinatorial background. There is also a hint for a peaking structure in the WS M_{miss}^* distribution, shown as a hatched histogram in Fig. 1(b). Due to $B^0 - \bar{B}^0$ oscillations, we expect a fraction of the produced B^0 mesons to decay as \bar{B}^0 given by $0.5x_d^2/(1+x_d^2) = 0.1861 \pm 0.0024$, where x_d is the B^0 mixing parameter [11].

Note that the momentum spectrum of B mesons produced in events with initial-state radiation (ISR), $e^+e^- \rightarrow \gamma BB$, overlaps significantly with that for B mesons from the three-body $e^+e^- \rightarrow B^{(*)}B^{(*)}\pi$ processes. However, ISR events do not produce peaking structures in the M_{miss}^* distribution.

A binned maximum likelihood fit is performed to fit the M_{miss}^* distribution to the sum of three Gaussian functions to represent three possible signals and two threshold components $A_k(x_k - x)^{\alpha_k} \exp\{(x - x_k)/\delta_k\}$ ($k = 1, 2$) to parameterize the $q\bar{q}$ and two-body $B^{(*)}\bar{B}^{(*)}$ backgrounds. The means and widths of the signal Gaussian functions are fixed from the signal MC simulation. The parameters A_k , α_k , δ_k of the background functions are free parameters of the fit; the threshold parameters x_k are fixed from the generic MC. ISR events produce an M_{miss}^* distribution similar to that for $q\bar{q}$ events; these two components are modeled by a single threshold function. The resolution of the signal peaks in Fig. 1(c) is dominated by the c.m. energy spread and is fixed at $6.5 \text{ MeV}/c^2$ as determined from the signal MC. The fit to the RS spectrum yields $N_{BB^*\pi} = 13 \pm 25$, $N_{B^*B^*\pi} = 357 \pm 30$ and $N_{B^*B^*\pi} = 161 \pm 21$ signal events. The statistical significance of the observed $BB^*\pi$ and $B^*B^*\pi$ signal is 9.3σ and 8.1σ , respectively. The statistical significance is calculated as $\sqrt{-2 \ln(\mathcal{L}_0/\mathcal{L}_{\text{sig}})}$, where \mathcal{L}_{sig} and \mathcal{L}_0 denote the likelihood values obtained with the nominal fit and with the signal yield fixed at zero, respectively.

For the subsequent analysis, we require $|M_{\text{miss}}^* - m_{B^*}| < 15 \text{ MeV}/c^2$ to select $BB^*\pi$ signal events and $|M_{\text{miss}}^* - (m_{B^*} + \Delta m_B)| < 12 \text{ MeV}/c^2$, where $\Delta m_B =$

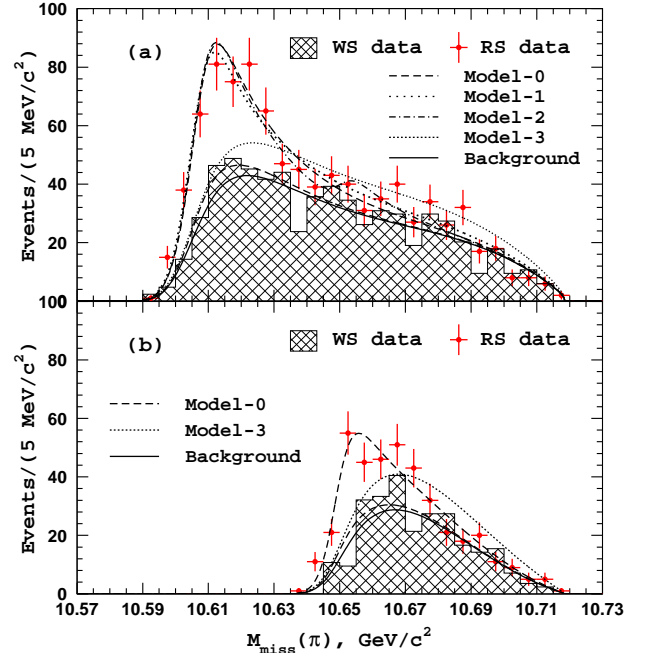


FIG. 2. The $M_{\text{miss}}(\pi)$ distribution for the (a) $BB^*\pi$ and (b) $B^*B^*\pi$ candidate events.

$m_{B^*} - m_B$, to select $B^*B^*\pi$ events. For the selected $B^*B^{(*)}\pi$ candidates, we calculate $M_{\text{miss}}(\pi) = \sqrt{(\sqrt{s} - E_{\pi})^2/c^4 - P_{\pi}^2/c^2}$, where E_{π} and P_{π} are the reconstructed energy and momentum, respectively, of the charged pion in the c.m. frame. The $M_{\text{miss}}(\pi)$ distributions are shown in Fig. 2 [12]. We perform a simultaneous binned maximum likelihood fit to the RS and WS samples, assuming the same number and distribution of background events in both samples and known fraction of signal events in the RS sample that leaks to the WS sample due to mixing. To fit the $M_{\text{miss}}(\pi)$ spectrum, we use the function

$$F(m) = [f_{\text{sig}}S(m) + B(m)]\epsilon(m)F_{\text{PHSP}}(m), \quad (1)$$

where $m \equiv M_{\text{miss}}(\pi)$; $f_{\text{sig}} = 1.0$ (0.1105 ± 0.0016 , [13]) for the RS (WS) sample; $S(m)$ and $B(m)$ are the signal and background PDFs, respectively; and $F_{\text{PHSP}}(m)$ is the phase space function. To account for the instrumental resolution, we smear the function $F(m)$ with a Gaussian function. The reconstruction efficiency is parameterized as $\epsilon(m) \sim \exp((m - m_0)/\Delta)(1 - m/m_0)^{3/4}$, where $m_0 = 10.718 \pm 0.001 \text{ GeV}/c^2$ is an efficiency threshold and $\Delta = 0.094 \pm 0.002 \text{ GeV}/c^2$.

The distribution of background events is parameterized as $B_{B^{(*)}B^*\pi}(m) = b_0 e^{-\beta \delta_m}$, where b_0 and β are fit parameters and $\delta_m = m - (m_{B^{(*)}} + m_{B^*})$. A general form of the signal PDF is written as

$$S(m) = |\mathcal{A}_{Z_b(10610)} + \mathcal{A}_{Z_b(10650)} + \mathcal{A}_{\text{nr}}|^2, \quad (2)$$

where $\mathcal{A}_{\text{nr}} = a_{\text{nr}} e^{i\phi_{\text{nr}}}$ is the non-resonant amplitude parameterized as a complex constant and the two Z_b

TABLE I. Summary of fit results to the $M_{\text{miss}}(\pi)$ distributions for the three-body $BB^*\pi$ and $B^*B^*\pi$ final states.

Mode	Parameter	Model-0	Model-1		Model-2		Model-3
			Solution 1	Solution 2	Solution 1	Solution 2	
$BB^*\pi$	$f_{Z_b(10610)}$	1.0	1.45 ± 0.24	0.64 ± 0.15	1.01 ± 0.13	1.18 ± 0.15	–
	$f_{Z_b(10650)}$	–	–	–	0.05 ± 0.04	0.24 ± 0.11	–
	$\phi_{Z_b(10650)}$, rad.	–	–	–	-0.26 ± 0.68	-1.63 ± 0.14	–
	f_{nr}	–	0.48 ± 0.23	0.41 ± 0.17	–	–	1.0
	ϕ_{nr} , rad.	–	-1.21 ± 0.19	0.95 ± 0.32	–	–	–
	$-2 \log \mathcal{L}$	–304.7	–300.6	–300.5	–301.4	–301.4	–344.5
$B^*B^*\pi$	$f_{Z_b(10650)}$	1.0	1.04 ± 0.15	0.77 ± 0.22	–	–	–
	f_{nr}	–	0.02 ± 0.04	0.24 ± 0.18	–	–	1.0
	ϕ_{nr} , rad.	–	0.29 ± 1.01	1.10 ± 0.44	–	–	–
	$-2 \log \mathcal{L}$	–182.4	–182.4	–182.4	–	–	–209.7

amplitudes, \mathcal{A}_{Z_b} , are parameterized with Breit-Wigner functions $\mathcal{A}_{Z_b} = a_Z e^{i\phi_Z} / (m^2 - m_Z^2 - i\Gamma_Z m_Z)$. The masses and widths of the Z_b states are fixed at the values obtained from the analyses of the $e^+e^- \rightarrow \Upsilon(nS)\pi^+\pi^-$ and $e^+e^- \rightarrow h_b(mP)\pi^+\pi^-$: $M_{Z_b(10610)} = 10607.2 \pm 2.0$ MeV/ c^2 , $\Gamma_{Z_b(10610)} = 18.4 \pm 2.4$ MeV and $M_{Z_b(10650)} = 10652.2 \pm 1.5$ MeV/ c^2 , $\Gamma_{Z_b(10650)} = 11.5 \pm 2.2$ MeV [1].

We first analyze of the $BB^*\pi$ [$B^*B^*\pi$] data with the simplest hypothesis, Model-0, that includes only the $Z_b(10610)$ [$Z_b(10650)$] amplitude. Results of the fit are shown in Fig. 2; the numerical results are summarized in Table I. The fraction f_X of the total three-body signal attributed to a particular quasi-two-body intermediate state is calculated as $f_X = \int |\mathcal{A}_X|^2 dm / \int S(m) dm$, where \mathcal{A}_X is the amplitude for a particular component X of the three-body amplitude. Next, we extend the hypothesis to include a possible non-resonant component, Model-1, and repeat the fit to the data. Then the $BB^*\pi$ data is fit to a combination of two Z_b amplitudes, Model-2. In both cases, the addition of an extra component to the amplitude does not give a statistically significant improvement in the data description: the likelihood value is only marginally improved (see Table I). The addition of extra components to the amplitude also produces multiple maxima in the likelihood function. As a result, we use Model-0 as our nominal hypothesis. Finally, we fit both samples to a pure non-resonant amplitude (Model-3). In this case, the fit is significantly worse.

If the parameters of the Z_b resonances are allowed to float, the fit to the $BB^*\pi$ data with Model-0 gives 10605 ± 6 MeV/ c^2 and 25 ± 7 MeV for the $Z_b(10610)$ mass and width, respectively, and the fit to the $B^*B^*\pi$ data gives 10648 ± 13 MeV/ c^2 and 23 ± 8 MeV for the $Z_b(10650)$ mass and width, respectively. The large errors here reflect the strong correlation between the resonance parameters.

The three-body visible [14] cross sections are calculated

as

$$\sigma_{\text{vis}}(e^+e^- \rightarrow f) = \frac{N_f}{L \cdot \mathcal{B}_f \cdot \alpha \cdot \eta}, \quad (3)$$

where N_f is the three-body signal yield and $L = 121.4$ fb $^{-1}$ is the total integrated luminosity. The efficiency-weighted sum of B -meson branching fractions \mathcal{B}_f is determined using both signal MC and two-body $e^+e^- \rightarrow B^{(*)}\bar{B}^{(*)}$ events in data. To avoid the large systematic uncertainties associated with the determination of reconstruction efficiencies for B and D decays to multibody final states, we select a subset of two-body modes: $B^+ \rightarrow \bar{D}^0[K^+\pi^-]\pi^+$ and $B \rightarrow J/\psi[l^+l^-]K$, and calculate $\mathcal{B}_f = \mathcal{B}_f^{\text{sel}} \times r \times N_{B^{(*)}\bar{B}^{(*)}}^{\text{all}} / N_{B^{(*)}\bar{B}^{(*)}}^{\text{sel}}$, where the superscripts “sel” and “all” refer to quantities determined for the selected subset of B decay modes and for the full set of modes, respectively. Two-body $e^+e^- \rightarrow B^{(*)}\bar{B}^{(*)}$ events are selected with the requirement 0.90 GeV/ $c < P(B) < 1.35$ GeV/ c ; the B yield is determined from the fit to the $M(B)$ distribution. We find $N_{B^{(*)}\bar{B}^{(*)}}^{\text{all}} = 10131 \pm 152$ and $N_{B^{(*)}\bar{B}^{(*)}}^{\text{sel}} = 2406 \pm 62$. To correct for a possible dependence of the B meson reconstruction efficiency on its momentum, we calculate the double ratio r using MC simulation: $r = (\mathcal{B}_{B^{(*)}\bar{B}^{(*)}}^{\text{sel}} / \mathcal{B}_{B^{(*)}\bar{B}^{(*)}}^{\text{all}}) / (\mathcal{B}_{B^{(*)}B^{(*)}\pi}^{\text{sel}} / \mathcal{B}_{B^{(*)}B^{(*)}\pi}^{\text{all}}) = 1.0017 \pm 0.0096$. To account for the non-uniform distribution of signal events over the phase space, we introduce an efficiency correction factor η determined from the MC simulation with signal events generated according to the nominal model. Since we do not observe a signal in the $BB\pi$ final state, no correction is made for this channel. A factor $\alpha = 0.897 \pm 0.007$ is introduced to correct for the effect of neutral B -meson oscillations that is determined using the known B^0 mixing parameter x_d and the yield ratio in data of three-body events with a reconstructed neutral vs. charged B meson. The results are summarized in Table II.

The dominant sources of systematic uncertainties for the three-body production cross sections are the uncertainties in the signal yield extraction (6.9% for $BB^*\pi$

TABLE II. Summary of results on three-body cross sections. The first (or sole) uncertainty is statistical; the second is systematic.

Parameter	$BB\pi$	$BB^*\pi$	$B^*B^*\pi$
Yield, Events	13 ± 25	357 ± 30	161 ± 21
$\mathcal{B}_f, 10^{-6}$	293 ± 22	276 ± 21	223 ± 17
η	1.0	1.066	1.182
$\sigma_{\text{vis}}, \text{pb}$	< 2.1	$11.2 \pm 1.0 \pm 1.2$	$5.61 \pm 0.73 \pm 0.66$

and 8.7% for $B^*B^*\pi$), in the reconstruction efficiency (7.6%) (including secondary branching fractions [11]), in the correction factor α (1%), and the uncertainty in the integrated luminosity (1.4%). The overall systematic uncertainties for the three-body cross sections are estimated to be 7.9%, 10.4%, and 11.7% for the $BB\pi$, $BB^*\pi$, and $B^*B^*\pi$ final states, respectively.

Using the results of the fit to the $M_{\text{miss}}(\pi)$ spectra with the nominal model (Model-0 in Table I) and the results of the analyses of $e^+e^- \rightarrow \Upsilon(nS)\pi^+\pi^-$ [1] and $e^+e^- \rightarrow h_b(mP)\pi^+\pi^-$ [15, 16], we calculate the ratio of the branching fractions $\mathcal{B}(Z_b(10610) \rightarrow B\bar{B}^* + c.c.)/\mathcal{B}(Z_b(10610) \rightarrow \text{bottomonium}) = 4.76 \pm 0.64 \pm 0.75$ and $\mathcal{B}(Z_b(10650) \rightarrow B^*\bar{B}^*)/\mathcal{B}(Z_b(10650) \rightarrow \text{bottomonium}) = 2.40 \pm 0.44 \pm 0.50$.

We calculate the relative fractions for Z_b decays, assuming that they are saturated by the already observed $\Upsilon(nS)\pi$, $h_b(mP)\pi$, and $B^*B^{(*)}$ channels. The results are summarized in Table III.

In conclusion, we report the first observations of the three-body $e^+e^- \rightarrow BB^*\pi$ and $e^+e^- \rightarrow B^*B^*\pi$ processes with a statistical significance above 8σ . Measured visible cross sections are $\sigma_{\text{vis}}(e^+e^- \rightarrow BB^*\pi) = (11.2 \pm 1.0 \pm 1.2)$ pb and $\sigma_{\text{vis}}(e^+e^- \rightarrow B^*B^*\pi) = (5.61 \pm 0.73 \pm 0.66)$ pb. For the $e^+e^- \rightarrow BB\pi$ process, we set a 90% confidence level upper limit of $\sigma_{\text{vis}}(e^+e^- \rightarrow BB\pi) < 2.1$ pb. The analysis of the $B^{(*)}B^*$ mass spectra indicates that the total three-body rates are dominated by the intermediate $e^+e^- \rightarrow Z_b(10610)^\mp\pi^\pm$ and $e^+e^- \rightarrow Z_b(10650)^\mp\pi^\pm$ transitions for the $BB^*\pi$ and $B^*B^*\pi$ final states, respectively.

We thank the KEKB group for excellent operation of the accelerator; the KEK cryogenics group for efficient solenoid operations; and the KEK computer group, the NII, and PNNL/EMSL for valuable computing and SINET4 network support. We acknowledge support from MEXT, JSPS and Nagoya's TLPSC (Japan); ARC and DIISR (Australia); FWF (Austria); NSFC (China); MSMT (Czechia); CZF, DFG, and VS (Germany); DST (India); INFN (Italy); MEST, NRF, GSDC of KISTI, and WCU (Korea); MNiSW and NCN (Poland); MES and RFAAE (Russia); ARRS (Slovenia); IKERBASQUE and UPV/EHU (Spain); SNSF (Switzerland); NSC and MOE (Taiwan); and DOE and NSF (USA).

TABLE III. B branching fractions for the $Z_b^+(10610)$ and $Z_b^+(10650)$ decays. The first quoted uncertainty is statistical; the second is systematic.

Channel	Fraction, %	
	$Z_b(10610)$	$Z_b(10650)$
$\Upsilon(1S)\pi^+$	$0.60 \pm 0.17 \pm 0.07$	$0.17 \pm 0.06 \pm 0.02$
$\Upsilon(2S)\pi^+$	$4.05 \pm 0.81 \pm 0.58$	$1.38 \pm 0.45 \pm 0.21$
$\Upsilon(3S)\pi^+$	$2.40 \pm 0.58 \pm 0.36$	$1.62 \pm 0.50 \pm 0.24$
$h_b(1P)\pi^+$	$4.26 \pm 1.28 \pm 1.10$	$9.23 \pm 2.88 \pm 2.28$
$h_b(2P)\pi^+$	$6.08 \pm 2.15 \pm 1.63$	$17.0 \pm 3.74 \pm 4.1$
$B^+\bar{B}^{*0} + \bar{B}^0B^{*+}$	$82.6 \pm 2.9 \pm 2.3$	—
$B^{*+}\bar{B}^{*0}$	—	$70.6 \pm 4.9 \pm 4.4$

- [1] A. Bondar *et al.* (Belle Collaboration), Phys. Rev. Lett. **108**, 122001 (2012).
- [2] A. Garmash *et al.* (Belle Collaboration), Phys. Rev. D **91**, 072003 (2015).
- [3] D.-Y. Chen and X. Liu, Phys. Rev. D **84**, 094003 (2011); A. Ali, C. Hambrock and W. Wang, Phys. Rev. D **85**, 054011 (2012); I. V. Danilkin, V. D. Orlovsky and Y. A. Simonov, Phys. Rev. D **85**, 034012 (2012); S. Ohkoda, Y. Yamaguchi, S. Yasui, K. Sudoh and A. Hosaka, Phys. Rev. D **86**, 014004 (2012); E. Braaten, C. Langmack and D. Hudson Smith, Phys. Rev. D **90**, 014044 (2014).
- [4] A. Bondar, A. Garmash, A.I. Milstein, R. Mizuk, and M.B. Voloshin, Phys. Rev. D **84**, 054010 (2011).
- [5] A. Drutskoy *et al.* (Belle Collaboration), Phys. Rev. D **81**, 112003 (2010).
- [6] A. Abashian *et al.* (Belle Collaboration), Nucl. Instrum. Methods Phys. Res. Sect. A **479**, 117 (2002); also see detector section in J. Brodzicka *et al.* Prog. Theor. Exp. Phys. (2012) 04D001.
- [7] S. Kurokawa and E. Kikutani, Nucl. Instrum. Methods Phys. Res. Sect. A **499**, 1 (2003), and other papers included in this Volume; T. Abe *et al.* Prog. Theor. Exp. Phys. (2013) 03A001 and following articles up to 03A011.
- [8] D.J. Lange, Nucl. Instrum. Methods Phys. Res. Sect. A **462**, 152 (2001).
- [9] R. Brun *et al.*, GEANT 3.21, CERN Report DD/EE/84-1, 1984.
- [10] T. Sjöstrand, Comput. Phys. Commun. **82**, 74 (1994).
- [11] K.A. Olive *et al.* (Particle Data Group), Chin. Phys. C, **38**, 090001 (2014).
- [12] The bin-by-bin information is available in the on-line supplementary material.
- [13] Determined using mixing parameter x_d and the ratio of charged to neutral B yields measured in data from two-body $e^+e^- \rightarrow B^{(*)}\bar{B}^{(*)}$ processes.
- [14] We do not apply an ISR correction here since the energy dependence of the cross section is not known.
- [15] I. Adachi *et al.* (Belle Collaboration), Phys. Rev. Lett. **108**, 032001 (2012).
- [16] The fits to the $M_{\text{miss}}(\pi)$ distributions performed in Ref. [1] give fractions of $f_{Z(10610)^\pm\pi^\mp} = 0.423^{+0.05+0.007}_{-0.127-0.009}$ ($0.352^{+0.156+0.001}_{-0.004-0.134}$) and $f_{Z(10650)^\pm\pi^\mp} = 0.602^{+0.103+0.11}_{-0.211-0.038}$

$(0.648_{-0.114}^{+0.152+0.067})$ for the $h_b(1P)$ ($h_b(2P)$) decays.

Supplementary Material

$M_{\text{miss}}(\pi)$ SPECTRA

In this supplementary material, we present the bin-by-bin information for the $M_{\text{miss}}(\pi)$ distribution shown in Fig. 2 of the Letter. Results are summarized in Table I, where the quoted uncertainty is statistical only. In addition to the right and wrong-sign yields, the detector relative efficiency is presented.

TABLE I: The three-body $B^{(*)}B^*\pi$ signal yields in $M_{\text{miss}}(\pi)$ bins.

$M_{\text{miss}}(\pi)$ bin, MeV/ c^2	$BB^*\pi$			$B^*B^*\pi$		
	RS data, Events	WS data, Events	Relative efficiency, Arbitrary units	RS data, Events	WS data, Events	Relative efficiency, Arbitrary units
10590 – 10595	1 ± 1.0	2.3 ± 1.7	0.937	–	–	–
10595 – 10600	15 ± 3.9	4.7 ± 2.4	0.958	–	–	–
10600 – 10605	38 ± 6.2	14.3 ± 4.1	0.979	–	–	–
10605 – 10610	64 ± 8.0	28.6 ± 5.8	0.999	–	–	–
10610 – 10615	81 ± 9.0	46.4 ± 7.4	1.017	–	–	–
10615 – 10620	75 ± 8.7	48.8 ± 7.6	1.034	–	–	–
10620 – 10625	81 ± 9.0	45.2 ± 7.3	1.050	–	–	–
10625 – 10630	65 ± 8.1	41.7 ± 7.0	1.064	–	–	–
10630 – 10635	47 ± 6.9	44.1 ± 7.2	1.075	–	–	–
10635 – 10640	45 ± 6.7	23.8 ± 5.3	1.084	1 ± 1.0	0.0 ± 1.1	1.084
10640 – 10645	39 ± 6.2	35.7 ± 6.5	1.089	11 ± 3.3	0.0 ± 1.1	1.089
10645 – 10650	43 ± 6.6	39.3 ± 6.8	1.091	21 ± 4.6	10.8 ± 3.6	1.091
10650 – 10655	40 ± 6.3	34.5 ± 6.4	1.089	55 ± 7.4	9.6 ± 3.4	1.089
10655 – 10660	31 ± 5.6	26.2 ± 5.6	1.082	45 ± 6.7	32.2 ± 6.2	1.082
10660 – 10665	35 ± 5.9	30.9 ± 6.1	1.070	46 ± 6.8	33.4 ± 6.3	1.070
10665 – 10670	40 ± 6.3	29.8 ± 5.9	1.051	51 ± 7.1	40.5 ± 6.9	1.051
10670 – 10675	27 ± 5.2	19.0 ± 4.7	1.025	43 ± 6.6	21.4 ± 5.0	1.025
10675 – 10680	34 ± 5.8	29.8 ± 5.9	0.991	32 ± 5.7	27.5 ± 5.7	0.991
10680 – 10685	26 ± 5.1	27.4 ± 5.7	0.946	21 ± 4.6	16.7 ± 4.4	0.946
10685 – 10690	32 ± 5.7	20.2 ± 4.9	0.891	18 ± 4.2	16.7 ± 4.4	0.891
10690 – 10695	17 ± 4.1	9.5 ± 3.4	0.821	20 ± 4.5	14.3 ± 4.1	0.821
10695 – 10700	18 ± 4.2	17.8 ± 4.6	0.735	11 ± 3.3	15.5 ± 4.3	0.735
10700 – 10705	8 ± 2.8	9.5 ± 3.4	0.629	9 ± 3.0	7.1 ± 2.9	0.629
10705 – 10710	8 ± 2.8	10.7 ± 3.6	0.495	5 ± 2.2	3.6 ± 2.1	0.495
10710 – 10715	6 ± 2.4	5.9 ± 2.7	0.322	5 ± 2.2	2.4 ± 1.7	0.322
10715 – 10720	2 ± 1.4	0.0 ± 1.1	0.056	1 ± 1.0	0.0 ± 1.1	0.056